Supporting Information

Perovskite lattice oxygen contributes to low-temperature catalysis for exhaust gas cleaning

Takuma Higo[a*], Kohei Ueno[a], Yuki Omori[a], Hiroto Tsuchiya[a], Shuhei Ogo[a], Satoshi Hirose[b], Hitoshi Mikami[b], Yasushi Sekine[a]

[a]Department of Applied Chemistry, Waseda University,
3-4-1, Okubo, Shinjuku, Tokyo 169-8555 Japan
[b]Honda R&D, 4630, Shimo-Takanezawa, Tochigi 321-3393 Japan

Table S1. NO conversion on $Pd/La_{0.9}Ba_{0.1}AlO_{3-\delta}$, $Pd/Ba/LaAlO_3$, $Pd/LaAlO_3$ and Pd/Al_2O_3. Reaction conditions: total flow rate = 200 mL min^{-1}, NO 1000 ppm, C_3H_6 500 ppm, O_2 2000 ppm, H_2O 7vol%.

Catalyst	473 K	523 K	573 K	623 K	673 K
Pd/Al_2O_3	0.5	7.4	31.7	54.2	50.6
$Pd/LaAlO_3$	0.6	6.1	18.1	40.1	50.6
$Pd/Ba/LaAlO_3$	0.4	12.3	28.3	43.2	52.6
$Pd/La_{0.9}Ba_{0.1}AlO_{3-\delta}$	4.4	34.9	42.3	48.1	48.5

Table S2. BET specific surface area of Pd/Al_2O_3, $Pd/LaAlO_3$, $Pd/Ba/LaAlO_3$ and $Pd/La_{0.9}Ba_{0.1}AlO_{3-\delta}$ catalysts.

Catalysts	BET specific surface area / m^2 g^{-1}	Mean particle diameter / nm	Turnover frequency / 10^{-2} s^{-1}
Pd/Al_2O_3	190.1	2.5	1.0
$Pd/LaAlO_3$	4.8	4.7	1.0
$Pd/Ba/LaAlO_3$	5.2	4.4	2.6
$Pd/La_{0.9}Ba_{0.1}AlO_{3-\delta}$	14.5	3.7	6.0

Table S3. NO conversion on $Pd/La_{0.9}Ba_{0.1}AlO_{3-\delta}$, $Pd/Ba/LaAlO_3$, $Pd/LaAlO_3$ and Pd/Al_2O_3. Reaction conditions: total flow rate = 200 mL min^{-1}, NO 2250 ppm, C_3H_6 250 ppm.

Catalyst	473 K	523 K	573 K	623 K	673 K
Pd/Al_2O_3	3.0	23.9	76.0	89.2	90.1
$Pd/LaAlO_3$	4.8	29.5	74.7	90.2	93.2
$Pd/Ba/LaAlO_3$	0.9	44.3	77.7	89.7	90.8
$Pd/La_{0.9}Ba_{0.1}AlO_{3-\delta}$	0.8	46.5	74.2	86.2	87.9

Table S4. NO conversion on $Pd/La_{0.9}Ba_{0.1}AlO_{3-\delta}$, $Pd/Ba/LaAlO_3$, $Pd/LaAlO_3$ and Pd/Al_2O_3. Reaction conditions: total flow rate = 200 mL min^{-1}, NO 1000 ppm, C_3H_6 500 ppm, O_2 2000 ppm.

Catalyst	473 K	523 K	573 K	623 K	673 K
Pd/Al_2O_3	8.1	15.3	32.4	47.9	55.1
$Pd/LaAlO_3$	1.9	8.6	22.6	48.4	50.0
$Pd/Ba/LaAlO_3$	3.1	23.6	37.3	49.9	58.4
$Pd/La_{0.9}Ba_{0.1}AlO_{3-\delta}$	12.6	40.4	55.1	56.3	60.8

Table S5. The amount of carbon dioxide species detected during transient response tests.

	$C^{16}O_2$ / μmol	$C^{16}O^{18}O$ / μmol	$C^{18}O_2$ / μmol
$Pd/Ba/LaAlO_3$	6.5	30.0	84.6

Table S6. Binding energy and surface atomic ratio of O1s region of XPS spectra for $Pd/Ba/LaAlO_3$.

Catalyst	Spectrum	Binding energy / eV				O_I/La	O_{II}/La	O_{III}/La	O_{IV}/La
		O_I	O_{II}	O_{III}	O_{IV}				
$Pd/Ba/LaAlO_3$	(d)	529.4	530.4	531.4	533.1	3.3	0.5	2.2	0.3
	(e)	529.3	530.4	531.5	533.4	2.7	1.0	2.2	0.3
	(f)	529.1	530.5	531.2	533.7	3.1	0.5	2.3	0.1

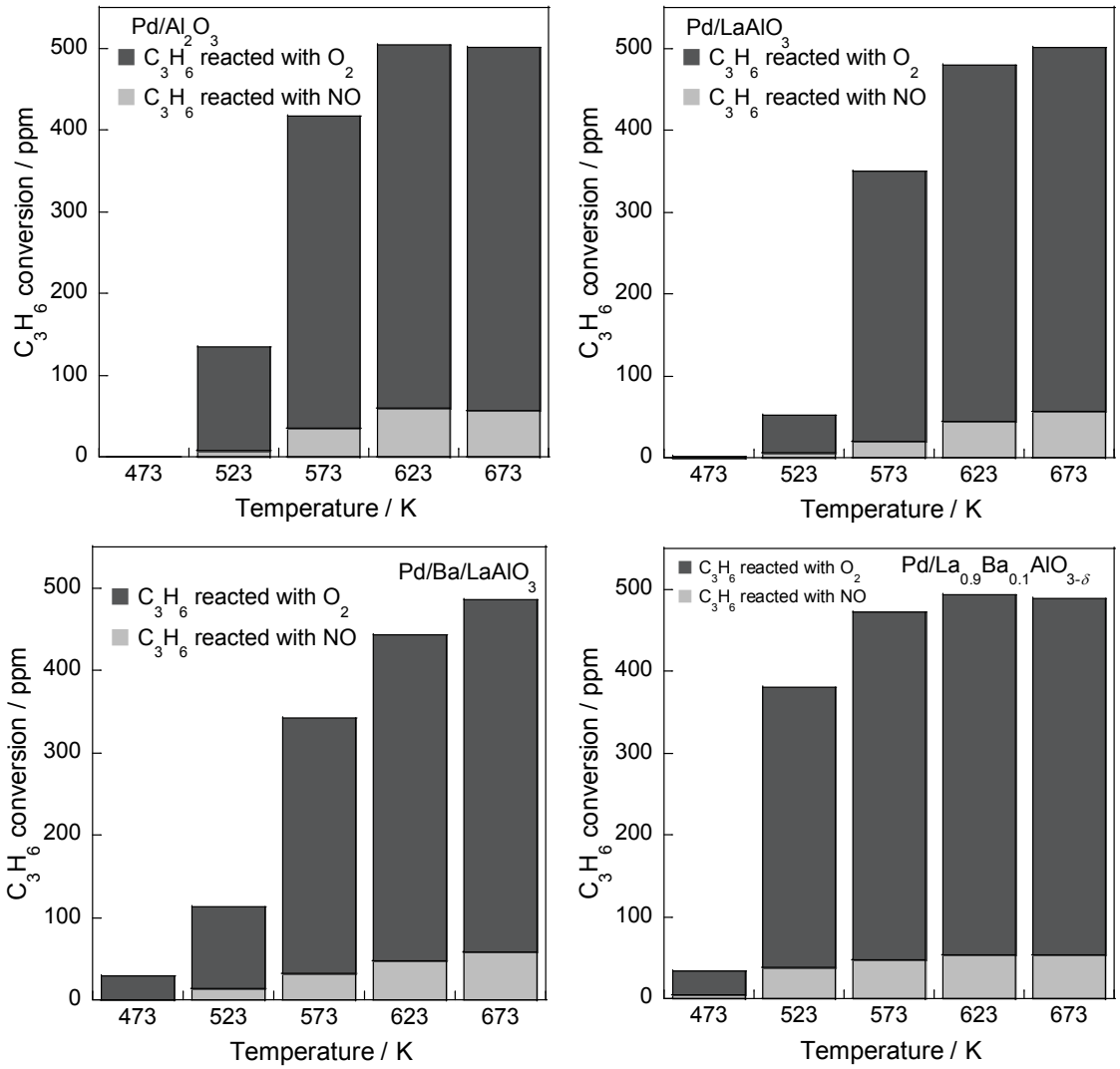

Figure S1. C_3H_6 conversion over $Pd/La_{0.9}Ba_{0.1}AlO_{3-\delta}$, $Pd/Ba/LaAlO_3$, $Pd/LaAlO_3$ and Pd/Al_2O_3. Reaction conditions: total flow rate = 200 mL min^{-1}, NO 1000 ppm, C_3H_6 500 ppm, O_2 2000 ppm, H_2O 7vol%.

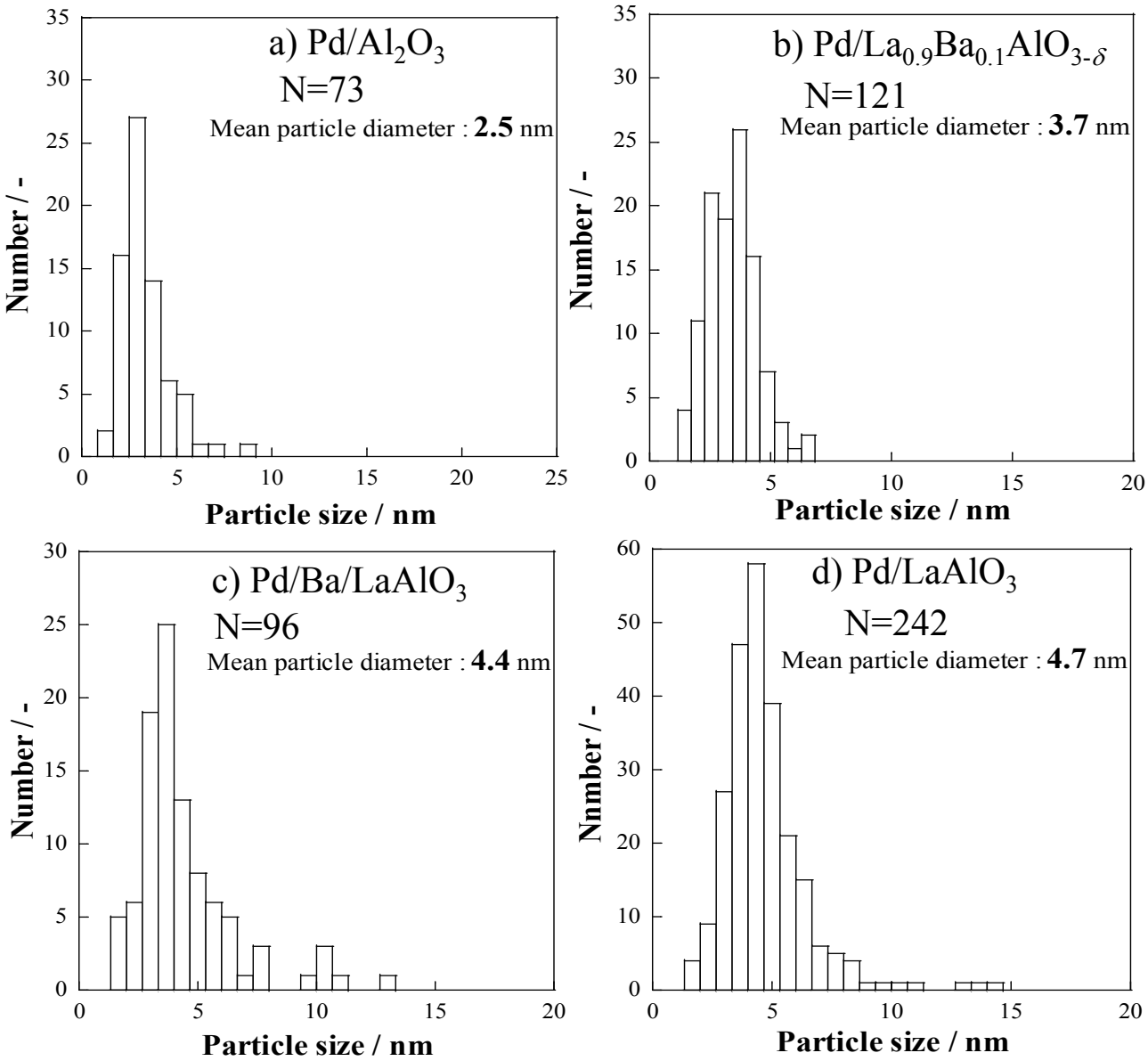

Figure S2. Distribution of Pd particle size on a) Pd/Al_2O_3, b) $Pd/La_{0.9}Ba_{0.1}AlO_{3-\delta}$, c) $Pd/Ba/LaAlO_3$ and d) $Pd/LaAlO_3$ catalysts.

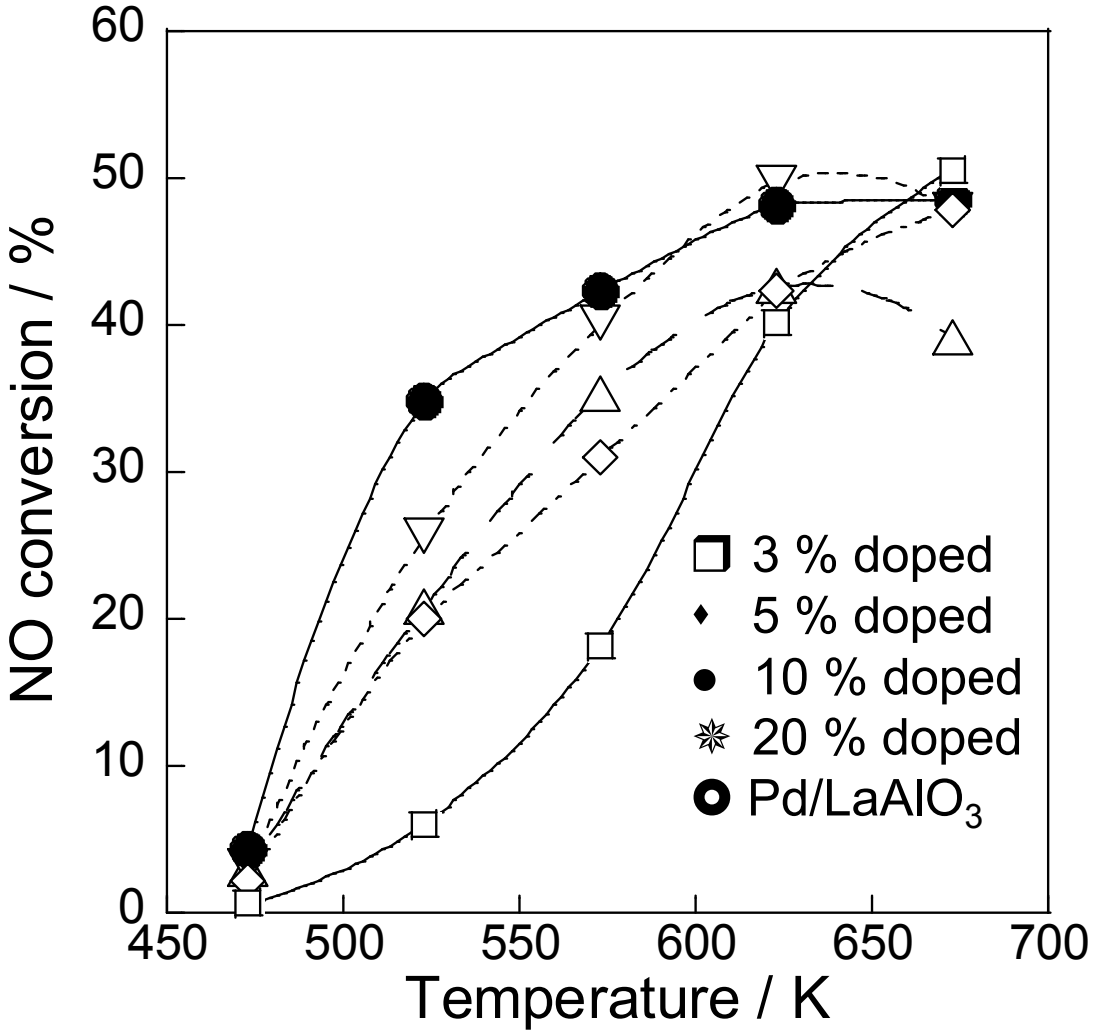

Figure S3. NO conversion over $Pd/La_{1-x}Ba_xAlO_{3-\delta}$ (x=0, 0.03, 0.05, 0.1, 0.2) catalysts.

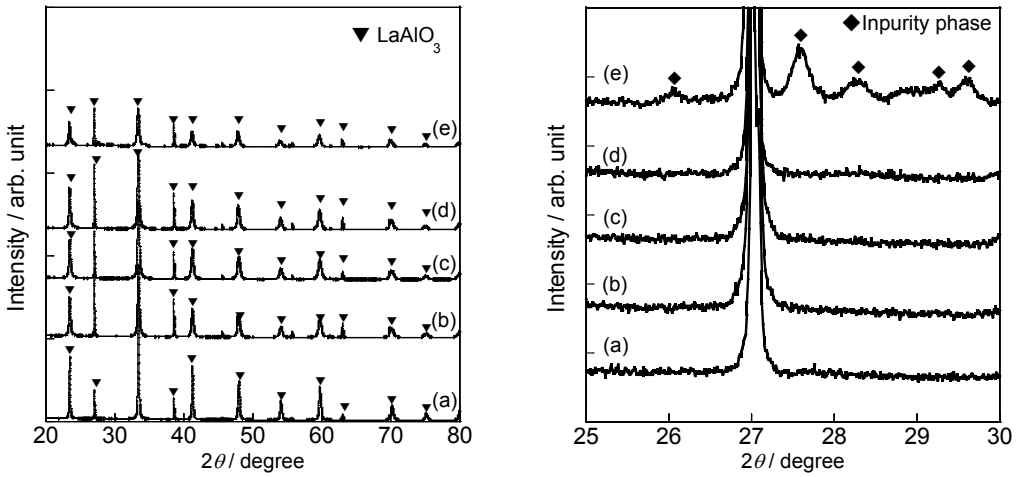

Figure S4. XRD patterns of (a) $LaAlO_3$, (b) $La_{0.97}Ba_{0.03}AlO_{3-\delta}$, (c) $La_{0.95}Ba_{0.05}AlO_{3-\delta}$, (d) $La_{0.9}Ba_{0.1}AlO_{3-\delta}$ and (e) $La_{0.8}Ba_{0.2}AlO_{3-\delta}$.

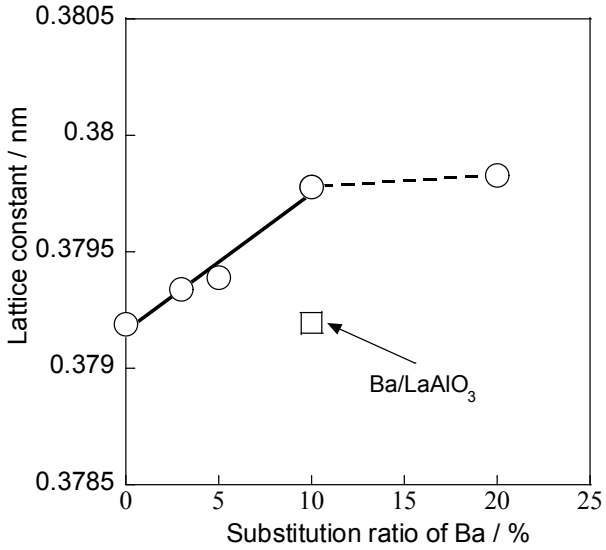

Figure S5. Lattice constant for $La_{1-x}Ba_xAlO_{3-\delta}$ and $Ba/LaAlO_3$.

For all Ba-substituted $LaAlO_3$ perovskites, main diffraction peaks were derived from $LaAlO_3$. Although these supports maintained the perovskite structure, impurity phases were observed on $Pd/La_{0.8}Ba_{0.2}AlO_{3-\delta}$, which showed low catalytic activity. Figure S5† shows the lattice constants for $La_{1-x}Ba_xAlO_{3-\delta}$ (x=0, 0.03, 0.05, 0.1 and 0.2) and $Ba/LaAlO_3$. Because the ionic radius of Ba is larger than that of La cation, the lattice constant of Ba substituted $LaAlO_3$ was distorted. As shown in Figure S5†, the lattice constant of $La_{1-x}Ba_xAlO_{3-\delta}$ catalysts monotonically increased as the increasing of Ba amount. From this result, it is inferred that Ba is substituted to a large extent into $LaAlO_3$ without deposition on the surface up to 10 % doping of Ba.

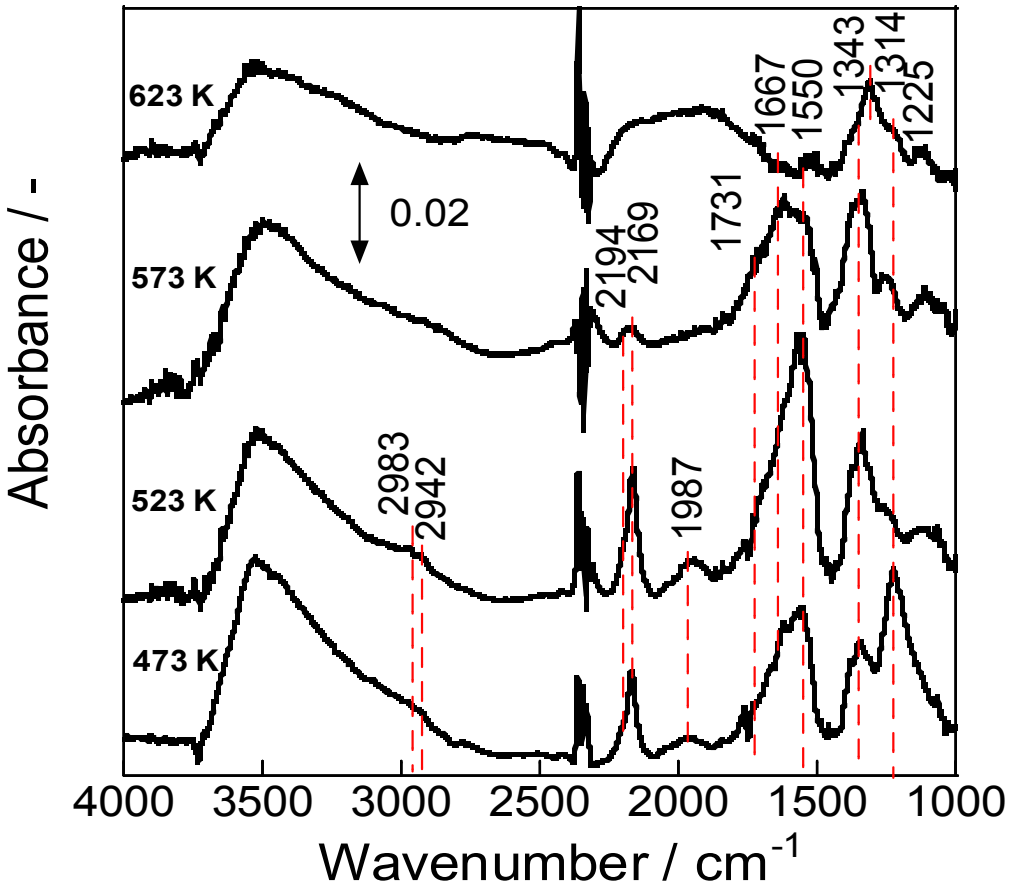

Figure S6. IR spectra of surface species on Pd/Ba/$LaAlO_3$ during NO-C_3H_6-O_2-H_2O reaction at 473-623 K.

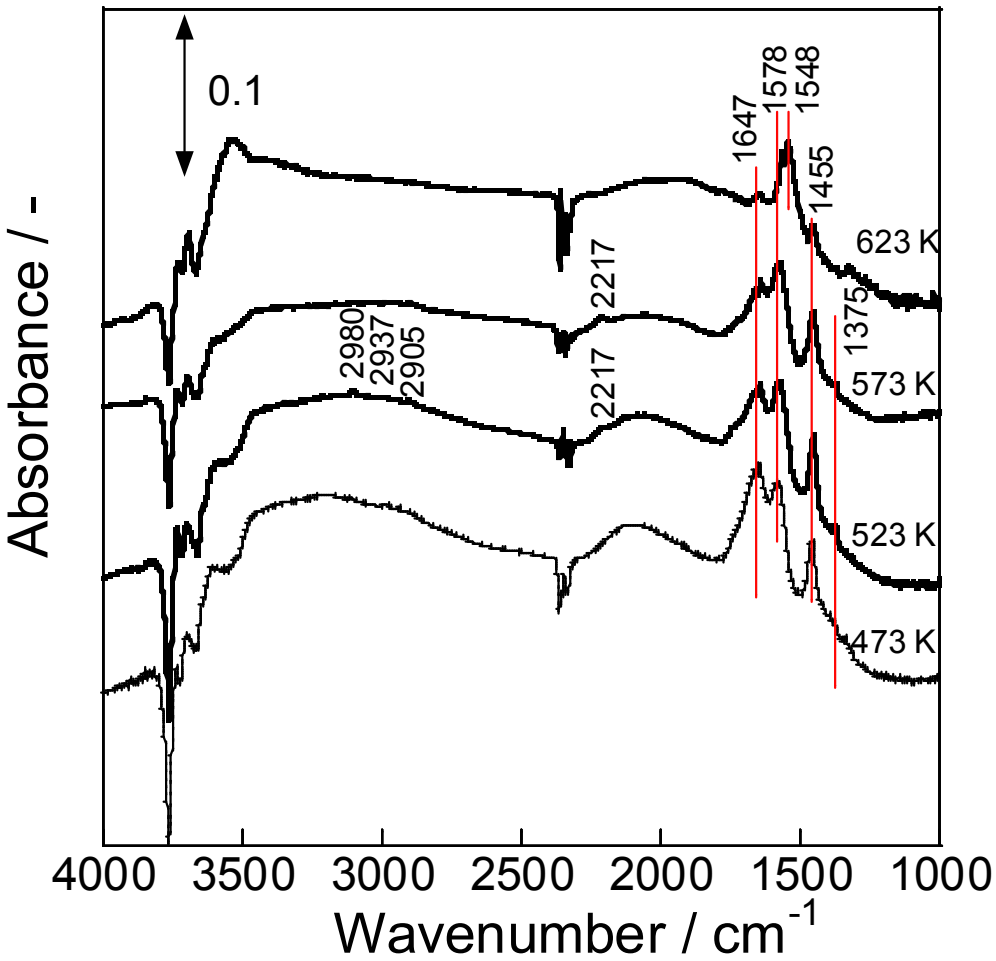

Figure S7. IR spectra of surface species on Pd/Al_2O_3 during $NO-C_3H_6-O_2-H_2O$ reaction at 473-623 K.

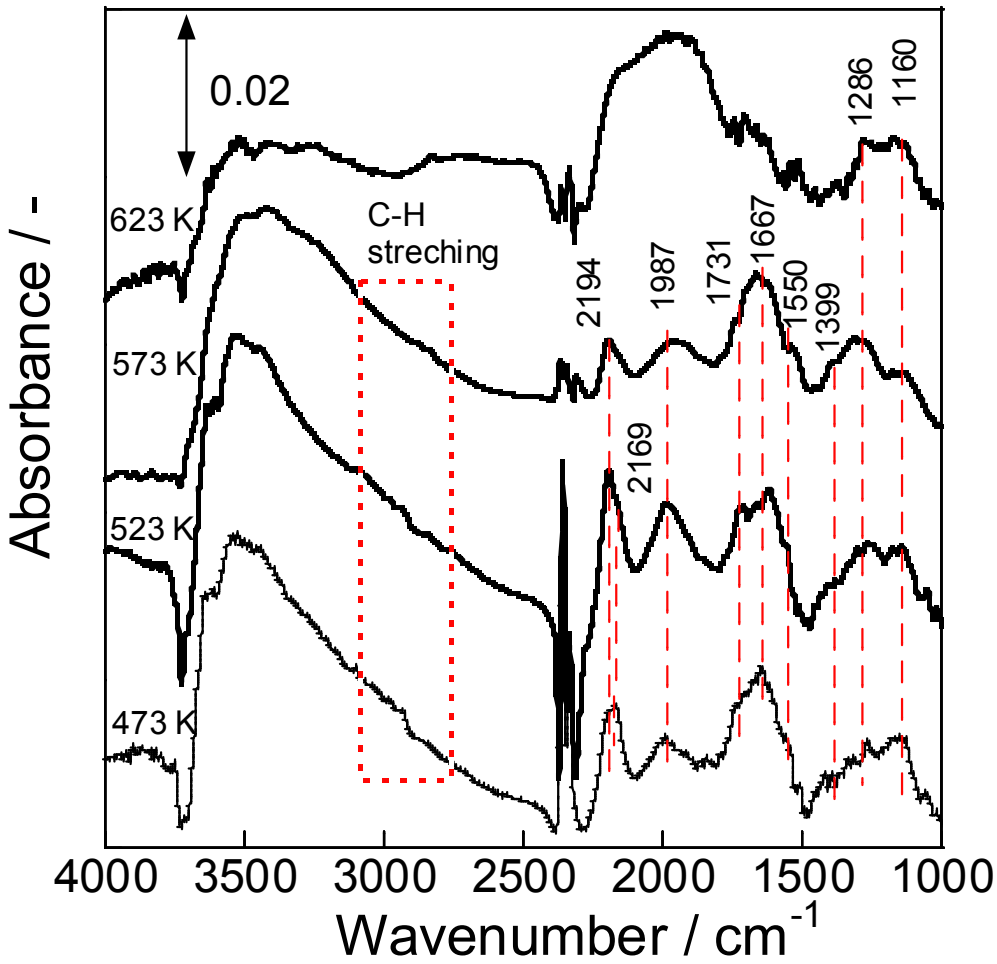

Figure S8. IR spectra of surface species on Pd/$LaAlO_3$ during NO-C_3H_6-O_2-H_2O reaction at 473 K-623 K.

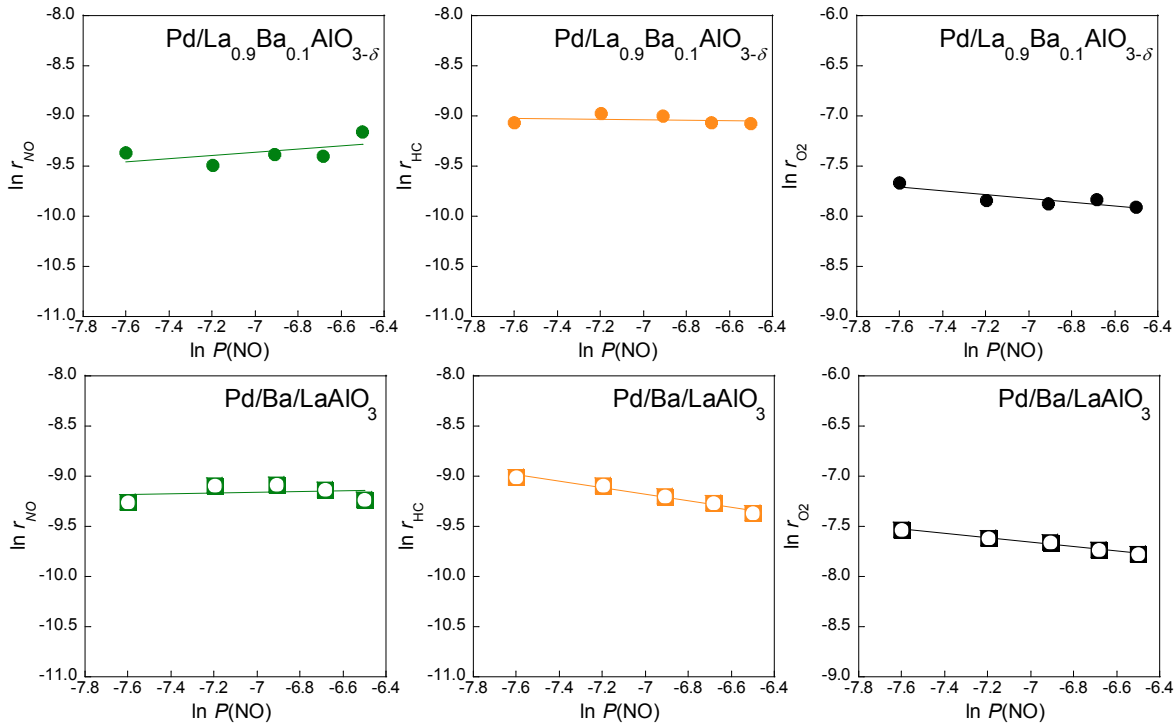

Figure S9. Dependence of the reaction rate on the partial pressure of NO on $Pd/La_{0.9}Ba_{0.1}AlO_{3-\delta}$ and $Pd/Ba/LaAlO_3$ at 523 K during $NO-C_3H_6-O_2-H_2O$ reaction.

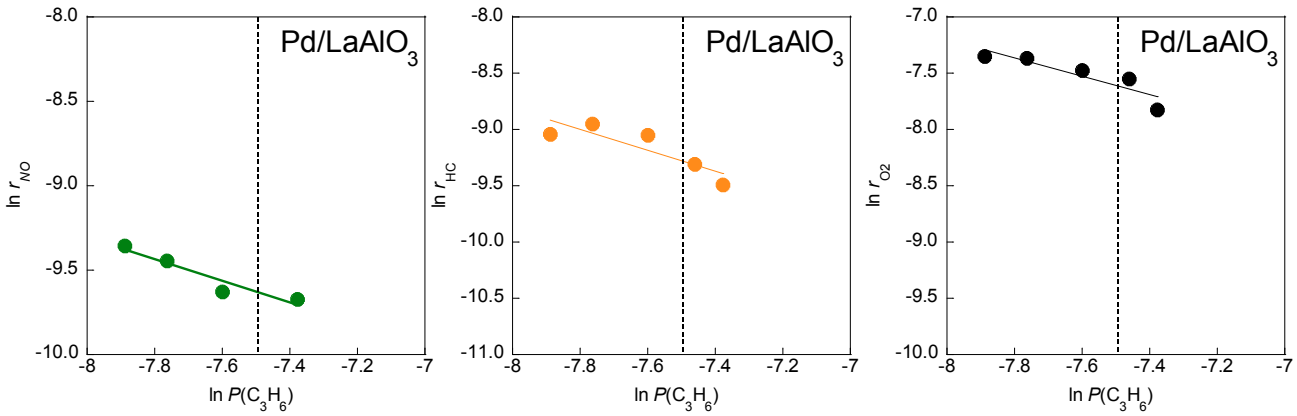

Figure S10. Dependence of the reaction rate on the partial pressure of C_3H_6 on $Pd/LaAlO_3$ at 523 K during NO-C_3H_6-O_2-H_2O reaction.

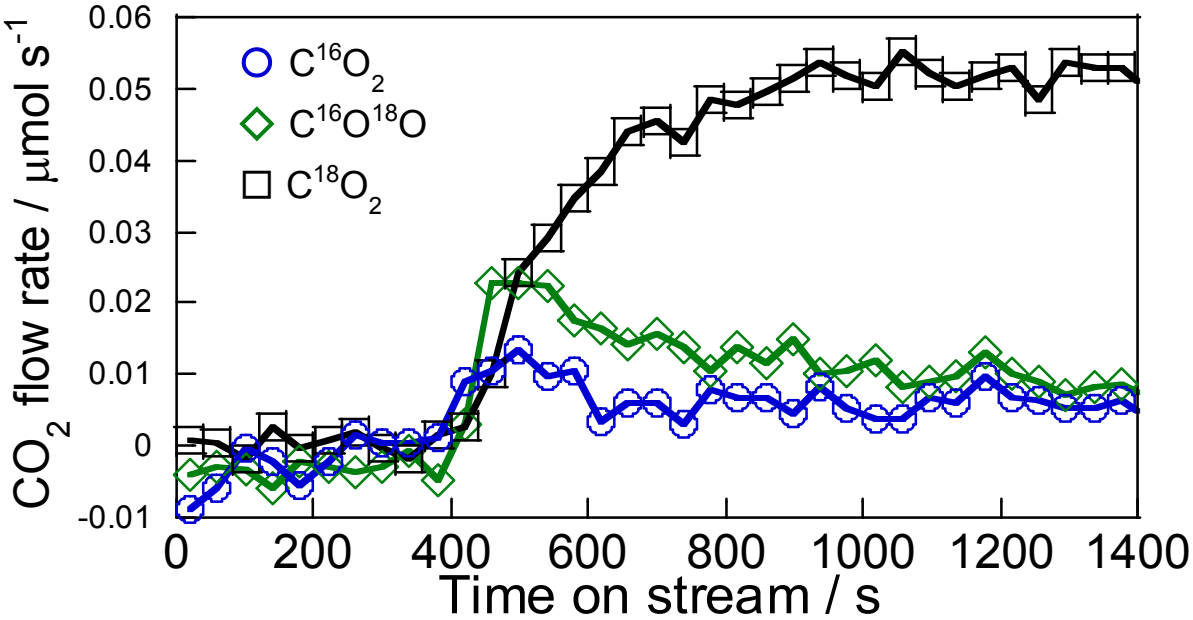

Figure S11. Transient response curves for typical products on Pd/Ba/$LaAlO_3$ following Ar → C_3H_6 + $^{18}O_2$ switch at 523 K.

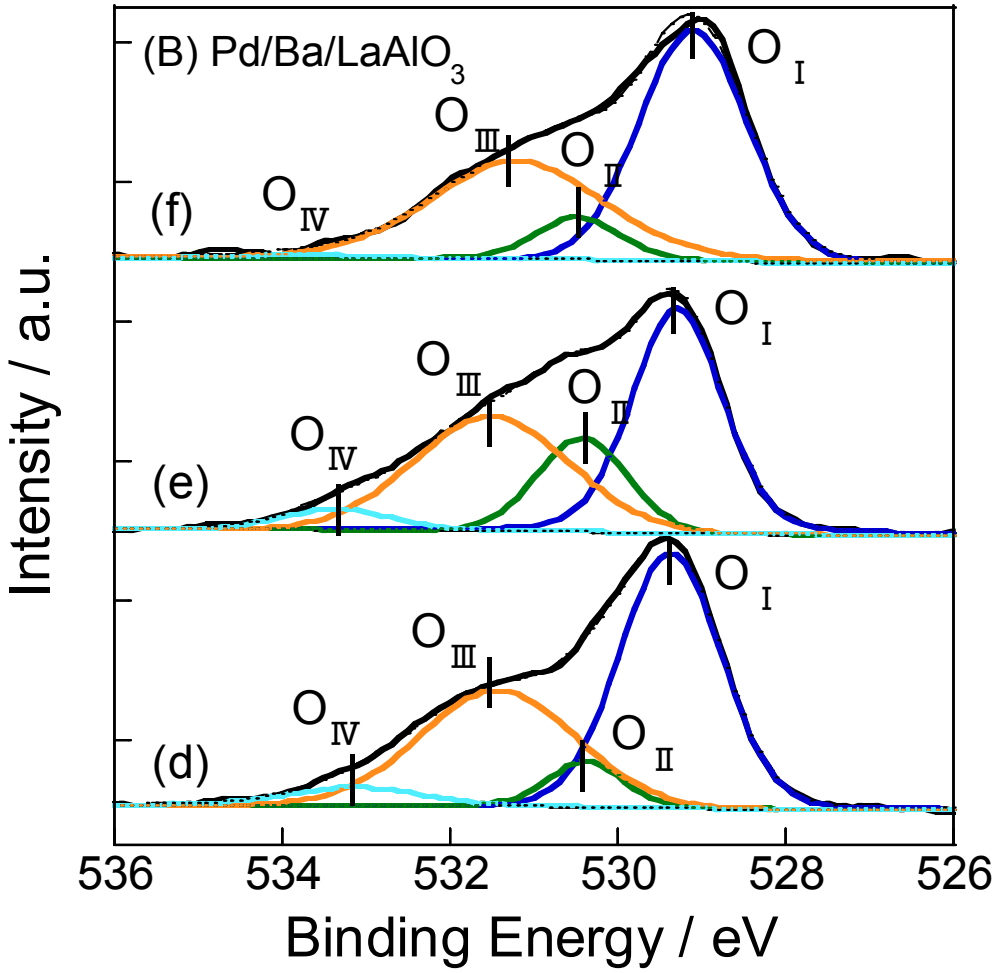

Figure S12. XPS spectra of O1s for Pd/Ba/$LaAlO_3$ (d) after exposure in C_3H_6 flow, (e) after exposure in O_2 and (f) after exposure of C_3H_6 flow again.

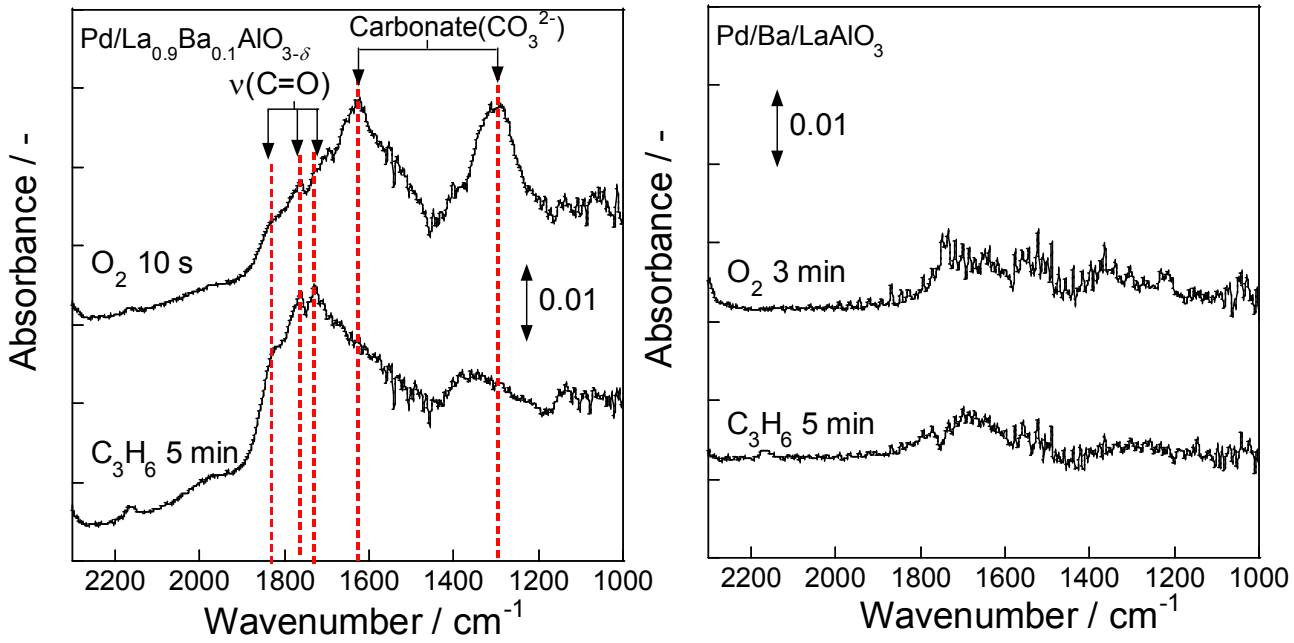

Figure S13. DRIFT spectra of $Pd/La_{0.9}Ba_{0.1}AlO_{3-\delta}$ and $Pd/Ba/LaAlO_3$ during second operation of transient test (switching from C_3H_6 to O_2 flow).